A structural comparative study of charge transfer compounds: Synthesis, crystal structure, IR, Raman-spectroscopy, DFT computation and hirshfeld surface analysis

Article *in* Journal of Molecular Structure · April 2019

DOI: 10.1016/j.molstruc.2019.04.084

7 authors, including:

Wahiba Falek
Abbes Laghrour - Khenchela University
12 PUBLICATIONS **18** CITATIONS
SEE PROFILE

Benali-Cherif Rim
17 PUBLICATIONS **15** CITATIONS
SEE PROFILE

Golea Lynda
science et technologie
5 PUBLICATIONS **12** CITATIONS
SEE PROFILE

Salima Samai
Abbes Laghrour - Khenchela University
2 PUBLICATIONS **0** CITATIONS
SEE PROFILE

Journal of Molecular Structure 1192 (2019) 132–144

Contents lists available at ScienceDirect

Journal of Molecular Structure

journal homepage: http://www.elsevier.com/locate/molstruc

A structural comparative study of charge transfer compounds: Synthesis, crystal structure, IR, Raman-spectroscopy, DFT computation and hirshfeld surface analysis

Wahiba Falek [a, b], Rim Benali-Cherif [b, *], Lynda Golea [c], Salima Samai [c], Nourredine Benali-Cherif [d, e, f], El-Eulmi Bendeif [g], Ismail Daoud [h, i]

[a] Département des Sciences de la matiére, Faculté des Sciences Exactes, des Sciences de la Nature et de la vie, Université "Larbi Ben Mhidi", Oum El Bouaghi, 04.000, Algeria
[b] Université Abbes Laghrour .40000, Khenchela, Algeria
[c] Laboratoire de Chimie et Chimie de l'Environnement (L.C.C.E), Département de Chimie, Faculté des Sciences de la matière, Université de Batna, Batna, 05000, Algeria
[d] Universite Akli Mohand Oulhadj-Bouira, Bouira, 10000, Algeria
[e] Ecole Nationale Polytechnique, Département de Génie des Matériaux, Constantine, 25000, Algeria
[f] Académie Algérienne des Sciences et Technologie (AAST), Algiers, Algeria
[g] Université de Lorraine, CNRS, CRM2, Nancy, France
[h] University Mohamed Khider, Department of Matter Sciences, BP 145 RP, 07000, Biskra, Algeria
[i] Laboratory of Natural and bio-actives Substances, Tlemcen University, Faculty of Science, P.O.Box 119, Tlemcen, Algeria

ARTICLE INFO

Article history:
Received 5 December 2018
Received in revised form
19 April 2019
Accepted 20 April 2019
Available online 24 April 2019

Keywords:
Charge transfer compounds
DFT calculation
X-ray diffraction
Intermolecular interactions
Structural analysis
Hirshfeld surface analysis

ABSTRACT

The present work focuses on the crystal structure analysis, vibrational spectroscopy investigation and DFT calculation. Two new charge transfer compounds; bis (creatininium) fumarate fumaric acid (**I**) and creatininium 3,5-dicarboxybenzoate monohydrate (**II**), have been synthesized, their Raman and IR modes of vibrations have been assigned and their crystal structures have been studied by means of single crystal X-ray diffraction. Complementary Hirshfeld surface analysis were carried out to investigate and quantify the contributions of the different intermolecular interactions within the crystal. This analysis revels that the main contributions in both compounds are provided by the O···H and H···H interactions that represent ~70 (for **I**) and ~75% (for **II**) of the total contributions to the Hirshfeld surface. The results of the theoretically predicted structural parameters and vibrational frequencies are in good agreements with the experimental investigations. These results show that both compounds exhibit similar features, however the energy gap between E_{HOMO} and E_{LUMO} obtained from the molecular orbital analysis indicates that compound **(I)** is characterized by a molecular structural more favourable for charge transfer.

1. Introduction

Creatinine (2-amino-1,5-dihydro-1-methyl-4H-imidazol-4-one) is an organic bio-molecule used in the synthesis of some charge transfer organic compounds [1], these organic compounds have also a predominant role in a wide range of chemical and biochemical processes such as solvation, catalytic, enzymatic reactions [2,3], and acid-base neutralization [4]. In addition, interesting properties such as non-linear optical (NLO) behaviour are sometimes the result of the strength and directionality of charge transfer interactions [5,6,7], they are also employed in optoelectronic materials elaboration [8,9]. Furthermore, organic ionic crystals are very promising materials and can be used as ingredients of choice for the development of new elaboration approaches. Moreover, photoinduced optical nonlinearity was also observed in ionic centrosymmetric crystals [10]. Although the development of creatininium salts continues to grow and a considerable number of research groups have gained great interest, a search in the Cambridge Structural Database CSD (ConQuest Version 1.23, 2018) [11] for crystal structures containing creatininium molecules results in 26 hits, 24 of them crystallize in a centrosymmetric space groupe.

* Corresponding author.
E-mail address: rym_46@hotmail.com (R. Benali-Cherif).

https://doi.org/10.1016/j.molstruc.2019.04.084
0022-2860/

All these interesting properties led us to the synthesis of novel creatinine charge transfer compounds. In this context, both trimesic and fumaric acids have been chosen to combine with creatinine, since they are excellent charge donors and formerly employed in the synthesis of some ionic crystals such as lithium fumarate [12], L-alaninium fumarate [13] and 4-dimethylaminopyridinium-3,5-dicarboxybenzoate trihydrate [14]. Owing to their interesting properties, trimesic acid and fumaric acid have been combined with creatinine to form two new organic materials; bis (creatininium) fumarate fumaric acid (**I**) and creatininium 3,5-dicarboxybenzoate monohydrate (**II**). We present in this work the following results: the structural parameters of the two salts (I) and (II) were characterized by FT-IR, Raman and, confirmed by single-crystal XRD studies. The graph-set descriptors of the intra- and intermolecular hydrogen bonding interactions stabilizing the two compounds were also reported and discussed. Intermolecular interactions have been examined by a complementary approach based on Hirshfeld surface analysis, which by means of the associated 2D fingerprint plots enabled similarities and differences in the crystal structures to be revealed. In addition, this research paper was complemented by theoretical calculations at the DFT level employing B3LYP/6-311 + G(d,p) basis sets. At the end, for understanding the molecular behaviour we calculated and visualized HOMO and LUMO using *Gaussian 09* and *GaussView* 5.0 software.

2. Experimental

2.1. Synthesis and crystallization

Compound (I): Creatinine (1.2 mmol) and an excess of fumaric acid (1.6 mmol) are dissolved separately in 20 ml of distilled water. The two solutions are mixed and stirred for 2 h. Single crystals were obtained after a few weeks, by slow evaporation at room temperature.

Compound (II): The same method is applied to trimesic acid (1.3 mmol) in slight excess, with the same amounts of creatinine (1.2 mmol) and water (20 ml). Single crystals appeared after a few weeks of slow evaporation at room temperature.

2.2. Single crystal X-ray diffraction and structure refinement details

The single crystal diffraction measurements were performed on an oxford Gemini diffractometer for compound **(I)** and on a Bruker D8 Venture diffractometer for compound **(II)**. Both experiments were carried out using Mo Kα radiation (λ = 0.71073 Å). Crystal data, data collection and structure refinement details of compounds (**I**) and (**II**) are summarized in Table 1. The structures have been solved by direct methods using the program *SIR*2011 [15] and were refined against F^2 by weighted full-matrix least squares methods including all reflections with *SHELXL*-2013 program [16]. All calculations were carried out using *WingX* software package [17]. Structural representations of the two salts were drawn using *MERCURY* [18]. All non-H atoms were refined anisotropically. The electron densities of all hydrogen atoms involved in strong intermolecular interactions were clearly identified in the difference density Fourier maps and their atomic coordinates and isotropic displacement parameters were refined. However, the remaining hydrogen atoms, namely those linked to the carbon atoms (C—H), have been treated with riding model.

2.3. Infra red and Raman spectroscopy

FT-IR spectra of both complexes were recorded by KBr pellet technique in the region of 4000–500 cm^{-1} with Bruker Optics IFS66v/s FT-IR spectrometer at a resolution of 2 cm^{-1}. Raman spectrum in the powder form was obtained using a Bruker Senterra Dispersive Raman microscope spectrometer with 532 nm excitation from a 3B diode laser having 2 cm^{-1} resolution in the spectral region of 3500–0 cm^{-1}

2.4. Computational details

The full geometrical optimization of structures (Fig. 1b and Fig. 4b) were carried out at density functional theory (DFT) [19] using a gradient technique [20,21] and 6-311 + G(d,p) [22,23] basis set. The DFT calculations were carried out with the B3LYP functional, in which Becke's nonlocal exchange [24,25] and the Lee-Yang-Parr correlation functional [26]. DFT calculations were performed using *GAUSSIAN 09* program package accessible in the *CPO* platform [27].

The nature of each stationary point was distinct by calculating harmonic vibrational frequencies. Every crystal structure has real frequencies. It must be indicated that the energies of all structures were attained using the DFT method and corrected for differences in zero-point vibrational energies scaled by 0.99 [28]. Calculated vibrational frequencies ensured that the structures were stable (with no imaginary frequencies) [29].

2.5. Hirshfeld Surface (HS) calculations

Molecular *HS* [30] in crystal structures have been constructed based on the electron distribution calculated as the sum of spherical atom electron densities [31]. For a given crystal structure and set of spherical atomic electron densities, the *HS* is unique [32]. This method is increasingly popular in a discussion of all existing interactions in the structure. The three dimensional *HS* and two-dimensional fingerprint plots of (**I**) and (**II**) were calculated using the *CrystalExplorer* program [33] and are mapped using the normalized contact distance (d_{norm}), which is calculated using the following formula:

$$d_{\mathrm{norm}} = \frac{d_i - r_i^{vdW}}{r_i^{vdW}} + \frac{d_e - r_e^{vdW}}{r_e^{vdW}}$$

The normalized contact distance (d_{norm}) is based on both (d_e) (distance from the point to the nearest nucleus external to the surface) and (d_i) (distance to the nearest nucleus internal to the surface), and the vdW radii of the atoms. It is also worth noting that *HS* maps are characterized by a red-blue-white color scheme: red region corresponds to a distance of intermolecular contacts less than van der Waal distance and negative value of d_{norm}; the blue region corresponds to a distance of intermolecular contacts higher than van der Waal distance and positive d_{norm} value; and the white region corresponds to the distance of contacts which is equally the van der waal distance and with a d_{norm} value of zero.

3. Results and discussion

3.1. Structural analysis

3.1.1. Structure and crystal packing of (I)

The asymmetric unit of (**I**) comprised one protonated creatininium cation $(C_4H_8N_3O)^+$, one-half of fumarate dianion $(0.5(C_4H_2O_4^{2-}))$ and one-half of fumaric acid $(0.5(C_4H_4O_4))$ (Fig. 1).

Bond distances and bond angles are comparable with those observed in similar compounds [34] (Table 2). Geometric environment of the imine (angles and distances) confirms its protonation on N1. Both the fumarate and the fumaric acid are centrosymmetric, the inversion center is at the midpoint of the C=

Table 1
Main crystallographic data and structure refinement details for compounds (**I**) and (**II**).

Crystal data	(I)	(II)
Empirical Formula	C_{16} H_{22} N_6 O_{10}	C_{13} H_{15} N_3 O_8
Molecular weight (g/mol)	458.40	341.28
Diffractometer,	Oxford Diffraction Gemini	Bruker D8 Venture
Radiation type	Mo Kα (λ = 0.71073 Å)	Mo Kα (λ = 0.71073 Å)
T (K)	293	100
Calculated density (g/cm^3)	1.503	1.570
Crystal system	Monoclinic	Triclinic
Space group	P 2_1/c	P −1
a (Å)	5.8987(7)	8.3963 (4)
b (Å)	21.7947(5)	8.6059 (4)
c (Å)	7.8782 (5)	10.8666 (5)
α (°)	90	79.167 (2)
β(°)	90.345 (2)	85.620 (4)
γ (°)	90	69.398 (3)
V (Å^3)	1012.81(14)	721.84 (6)
Z	2	2
μ (mm^{-1})	0.126	0.132
Crystal size (mm)	0.75 × 0.51 × 0.27	0.40 × 0.15 × 0.14
$T_{minimum}$, $T_{maximum}$	0.988, 0.994	0.964,0.975
No. of measured, independent and observed [I > 2σ(I)] reflections	3604, 2105, 1378	11858, 2944, 2386
R_{int}	0.024	0.038
$(\sin\theta/\lambda)_{maximum}$ (Å^{-1})	0.685	0.625
Refinement		
R[F^2 > 2σ(F^2)], w*R*(F^2), S	0.065, 0.177, 1.10	0.037, 0.096, 1.03
No. of unique reflections	2105	2944
No. of parameters	189	277
H-atom treatment	All H-atom parameters refined	All H-atom parameters refined
$\Delta\rho_{max}$, $\Delta\rho_{min}$	0.20, −0.26	0.23, −0.28

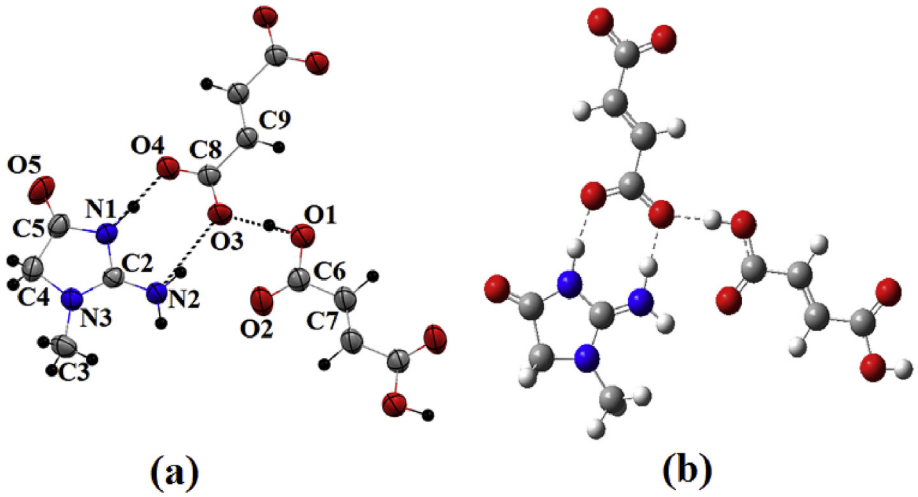

Fig. 1. **(a)** View of the ionic structure of (**I**), showing the immediate hydrogen-bonded between creatininium, fumarate and fumaric acid. Displacement ellipsoids are drawn at the 50% probability level and H atoms are shown as small black spheres of arbitrary radius. **(b)** Optimized molecular structure of (**I**).

C double bond. The fumarate anion was dually deprotonated and it was confirmed from —COO$^-$ bond geometry (d (C8 ⎓ O4) = 1.252 (4).

Å, d (C8 ⎓O3) = 1.256 (4) Å). The crystal structure of (**I**) (Figs. 1S and 2) can be described by an alternation of fumarate anions, creatininium cations and fumaric acids along *b*-axis. The creatininium entities are bonded together via one N—H···O hydrogen bond (Symmetry code: *x*+1, −*y*+1/2, *z*+1/2) (see Table 3). Six-membered $C_1^1(6)$ infinite chains parallel to ***a***-axis are built up from combination of these cation-cation interactions (Fig. 2) This is the third time in which creatininium cations are linked directly together via a hydrogen bond in all compounds reported in the CSD [11] and containing creatininium cation; the two first cases were observed in creatininium dihydrogenarsenate [35] and Creatininium tetrakis (3,5 bis(trifluoromethyl)phenyl)borate monohydrate [36] compounds (CSD refcodes: FONFIY and FAJNIQ respectively). Cations were found to be linked to anions forming ion pairs through two hydrogen bonds; one via the imino group N1 atom, thus forming strong interactions (2.605 (3) Å) along *b*-axis, and another via the amino N2 atoms, these two interactions produce $R_2^2(8)$ ring motifs [37] (Fig. 2). Carboxylate groups of fumarate and carboxyl groups of fumaric acids are hydrogen bonded through a very strong O—H···O (O1—H1···O3 = 2.555(4) Å) interaction leading to the formation of a one-dimensional hydrogen-bonded supramolecular twisting chain parallel to the crystallographic ***a***-axis, the association of these interactions gives rise to an infinite seven membered chains described by the $C_1^1(7)$ graph set along the same axis (Fig. 2). This type of carboxyl-carboxylate hydrogen bond has been reported in

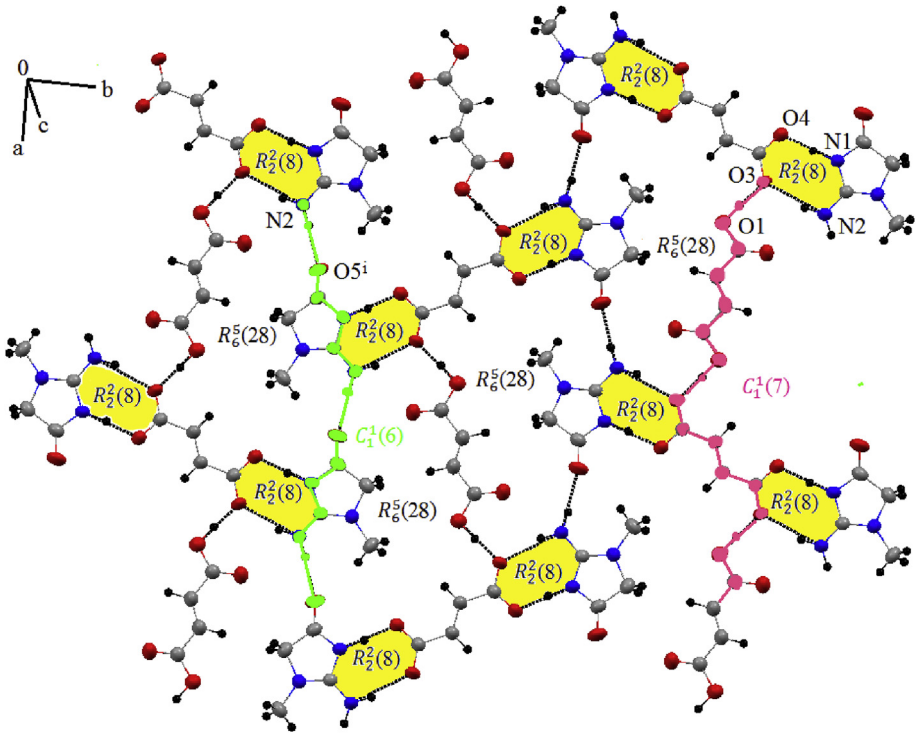

Fig. 2. View of the crystal packing of (**I**), illustrating the formation of $R_2^2(8)$ and $R_6^5(28)$ ring motifs and $C_1^1(6)$ (drawn in pink) and $C_1^1(7)$ (drawn in green) infinite chains.

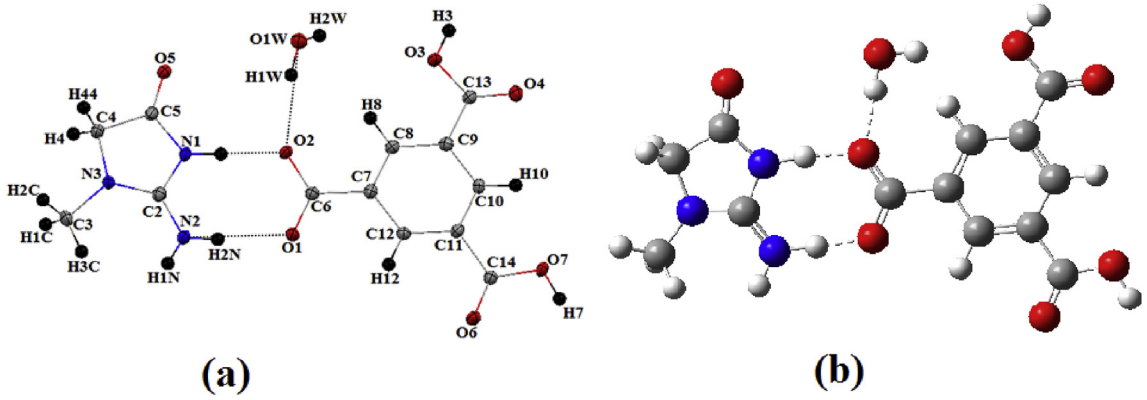

Fig. 3. **(a)** The asymmetric unit of (**II**), showing the atom-labelling scheme. Displacement ellipsoids are drawn at the 50% probability level and H atoms are shown as small black spheres of arbitrary radius. **(b)** Optimized molecular structure of (**II**).

several crystal structures containing fumarate-fumaric acid species with different cations [38–40] indicating the stability of such a supramolecular motif. These two cationic and anion-fumaric acids chains give rise to $R_6^5(28)$ ring motifs (Fig. 2).

3.1.2. Structure and crystal packing of (II)

The molecular structure of (**II**) consists of one creatininium cation $(C_4H_8N_3O)^+$, one 3,5-dicarboxybenzoate anion and one water molecule in its asymmetric unit (Fig. 3). The carboxyl proton at C6 of the benzene 1,3,5-tricarboxylic acid was transferred to a creatinine molecule which is confirmed by the presence of almost equal C–O bond lengths (1.2515 (18) Å, C6–O1 and 1.2708 (17) Å C6–O2) due to the existence of resonance in carboxylate ion [41,42]. As previously observed in (**I**), the creatinine base is also monoprotonated at the N1 imino group; this is also reflected in enlargement of the C–N–C angle [110.59 (12)°] compared to C–N–C angle in the creatinine molecule (107°) [43]. This protonation enlarges C–N–C angle by +3.59° (see Table 2). The crystal structure of (**II**) can be described as being composed of cation chains and anion molecules extending along ***b***-axis by forming layers parallel to [101] direction, alternating with water molecules-stacked layers along ***b***-axis (Fig. 2Sa and 2Sb). Creatininium cations are linked to anions forming dimers through two N–H···O intermolecular hydrogen bonds that produced $R_2^2(8)$ ring motif (Fig. 4). Like compound (**I**) the imino groups N1 atoms form strong interactions (2.6007(15) Å) parallel to the diagonal [011]. Cations and anions are also connected via one strong O–H···O hydrogen bond, this type of interaction creatininium-anions was never be observed, and this is the first case in which creatininium cation acts as a hydrogen bonding acceptor with anion via exocyclic carbonyl O5 atom by forming a strong hydrogen bond (O7–H7···O5 = 2.6455(14) Å), symmetry code: (iv) $x-1, y, z+1$ (see Table 3). Furthermore, the crystalline device is also maintained by a very strong O–H···O (O3–H3···O1 = 2.5699(15) Å) hydrogen bond

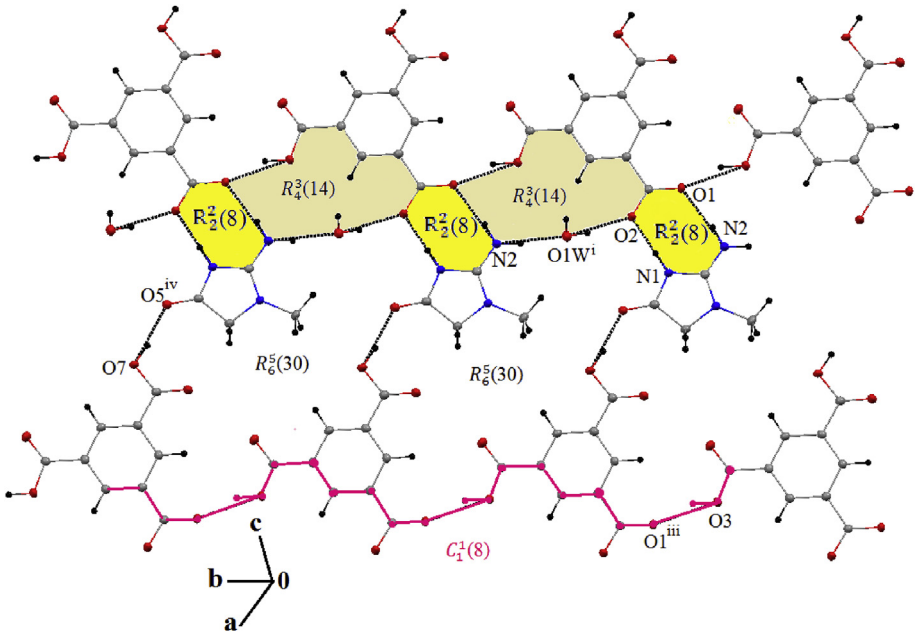

Fig. 4. A fragment of the (**II**) structure showing the graph set describing the hydrogen bonding ($R_2^2(8)$, $R_4^3(14)$ and $R_6^5(30)$ ring motifs are colored in yellow, brown and white respectively and $C_1^1(8)$ infinite chain is drawn with pink).

Table 2
Selected structural parameters, bond lengths (Å) and bond angles (°) for (**I**) and (**II**).

Compound (I)	Bond lengths (Å)	Bond angles (°)	Compound (II)	Bond lengths (Å)	Bond angles (°)
O4–C8	1.252 (4)	–	O1–C6	1.2515 (18)	–
O1–C6	1.318 (4)	–	O2–C6	1.2708 (17)	–
O3–C8	1.256 (4)	–	O3–C13	1.3273 (18)	–
N3–C2	1.316 (4)	–	O4–C13	1.2156 (18)	–
N3–C4	1.448 (4)	–	N1–C5	1.3668 (18)	–
N1–C5	1.355 (4)	–	N1–C2	1.369 (2)	–
N1–C2	1.374 (4)	–	N3–C2	1.3312 (19)	–
O2–C6	1.191 (4)	–	N3–C4	1.4587 (19)	–
C5–C4	1.503 (5)	–	C5–N1–C2	–	110.59 (12)
C2–N3–C4	–	110.1 (3)	C2–N3–C4	–	109.95 (12)
C5–N1–C2	–	109.8 (3)	N3–C2–N1	–	110.58 (13)
N3–C2–N1	–	110.7 (3)	N3–C4–C5	–	102.31 (11)
N1–C5–C4	–	107.2 (3)	O5–C5–N1	–	124.85 (13)
N3–C4–C5	–	102.2 (3)			

Table 3
Hydrogen bond lengths (Å) and angles (°).

D—H···A	D—H	H—A	D—A	D—H···A
Compound (I)				
O1–H1···O3	0.96(2)	1.59(2)	2.555(4)	175(5)
N1–H1N···O3	0.98(2)	2.58(4)	3.207(3)	122(3)
N1–H1N···O4	0.98(2)	1.63(2)	2.605(3)	173(4)
N2–H2N···O3	0.92(1)	1.96(1)	2.863(4)	167(4)
N2–H3N···O5^{i}	0.92(1)	1.96(2)	2.863(4)	166(6)
Compound (II)				
N1–H1N···O2	0.95(2)	1.65(2)	2.6007(15)	177(2)
N2–H3N···O1W^{i}	0.92(1)	1.95(1)	2.824(17)	158(2)
O1W–H1W···O2	0.93(2)	1.94(2)	2.8563(16)	171(2)
N2–H2N···O1	0.91(1)	1.95(1)	2.8627(16)	173(2)
O1W–H2W···O4^{ii}	0.93(2)	1.99(2)	2.8913(16)	164(2)
O3–H3···O1^{iii}	0.95(2)	1.67(2)	2.5699(15)	157(2)
O7–H7···O5^{iv}	0.94(2)	1.71(2)	2.6455(14)	172(2)
C3–H1C···O6^{v}	0.96(2)	2.57(2)	3.4924(19)	161(2)
C3–H3C···O1W^{i}	0.96(2)	2.59(2)	3.4760(19)	153(2)

Symmetry codes [compound (**I**)]: (i) $x+1, -y+1/2, z+1/2$.
Symmetry codes [compound (**II**)]: (i) $x, y-1, z$; (ii) $-x, -y+2, -z+1$; (iii) $x, y+1, z$; (iv) $x-1, y, z+1$; (v) $-x+1, -y, -z+1$.

established between anions parallel to ***b***-axis. The combination of these anion-anion hydrogen bonds gives rise to an infinite eight-membered chain described by the $C_1^1(8)$ graph set along the same direction (Fig. 4). The packing is a superposition of two types of bilayers: bilayer **1** and **2**, with and without water molecule respectively (Fig. 2Sb). This mode of stacking was observed in cytosine and 1,3,5, -tricarboxylic acid compound [44]. Water molecules play a role in the three-dimensional network of hydrogen bonding, they maintain cohesion in bilayers 1. O1W acting as hydrogen -bond acceptor and as a double hydrogen -bond donor (see Fig. 2Sa and Table 3). A detailed examination of the molecular packing reveals that the interlayer spacing in bilayer **1** [3.266 (2) Å] is slightly larger than that in bilayer **2** (3.181 (2) Å) (Fig. 2Sa).

In summary the structural investigation shows that the inspection of the hydrogen bonding network in both salts shows a direct hydrogen-bond interaction between the creatininium cation and the fumarate (3,5-dicarboxybenzoate) anion. The (N–H···O) hydrogen bonds that connect anions and the imino groups N1 atoms in (**I**) and (**II**) are strong, while those that connect anions and the amino N2 atoms in (**I**) and (**II**) are of moderate strength. In both

Table 4
Geometric parameters as determined by X-ray crystallography and theoretical calculations for (**I**) and (**II**) using DFT - B3LYP/6-311 + G(d,p).

(I)	X-Ray	DFT	(II)	X-Ray	DFT
Bond lengths (Å)			**Bond lengths (Å)**		
O4–C8	1.252(4)	1.249	O2–C6	1.2708(17)	1.269
O3–C8	1.256(4)	1.274	O1–C6	1.2515(18)	1.252
C9–C8	1.489(4)	1.451	C6–C7	1.5099(19)	1.511
C9–C9	1.301(7)	1.331	C7–C8	1.388(2)	1.391
C9–H9	0.959(10)	1.081	C9–C13	1.487(2)	1.484
O1–H1	0.96(2)	1.041	C11–C14	1.497(19)	1.489
C6–O1	1.318(4)	1.523	C14–O7	1.3368(17)	1.353
C6–O2	1.191(4)	1.201	C14–O6	1.207(18)	1.208
C6–C7	1.473(5)	1.477	C13–O3	1.327(18)	1.352
C7–C7	1.262(8)	1.251	C13–O4	1.215(18)	1.221
O1–H1	0.96(2)	1.019	O3–H3	0.954(16)	0.961
C7–H7	0.961(10)	1.081	O7–H7	0.939(16)	0.966
N3–C2	1.316(4)	1.341	C10–H10	0.930(18)	1.082
N2–C2	1.307(4)	1.308	C8–H8	0.930(18)	1.087
N1–C2	1.374(4)	1.361	O1W–H1W	0.928(16)	0.971
N3–C4	1.448(4)	1.457	O1W–H2W	0.926(16)	0.961
N1–C5	1.355(4)	1.391	N2–H2N	0.913(10)	1.011
C5–O5	1.210(4)	1.199	N2–C2	1.311(2)	1.31
N3–C3	1.458(4)	1.452	N3–C2	1.331(19)	1.353
N1–H1N	0.980(19)	1.069	N3–C4	1.4587(19)	1.455
N2–H2N	0.917(10)	1.051	C4–C5	1.516(2)	1.532
N2–H3N	0.917(10)	1.011	C5–O5	1.221(18)	1.222
C3–H3C	0.960(8)	1.091	N3–C3	1.457(2)	1.451
C3–H3B	0.960(8)	1.092	C3–H2C	0.960(2)	1.091
C3–H3A	0.960(8)	1.092	C2–N1	1.369 (2)	1.351
Bond angles (°)			**Bond angles (°)**		
O4–C8–O3		125.31	O1–C6–O2	123.86(13)	125.01
C8–C9–C9	122.7(3)	121.86	C7–C6–O1	119.36(13)	117.26
C8–C9–H9	123.2(4)	117.14	C7–C12–C11	119.99(14)	120.57
C9–C9–H9	116(2)	120.78	C12–C11–C10	120.32(13)	119.77
C9–C8–O3	121(2)	123.21	C11–C10–C9	119.74(13)	119.86
C9–C8–O4	117.7(3)	120.25	C10–C9–C13	119.02(13)	117.52
O2–C6–O1	119.6(3) 124.2(3)	125.51	C9–C13–O3	113.05(12)	112.82
C6–C7–C7	125.9(4)	123.26	H3–O3–C13	114.3(14)	110.46
C6–O1–H1	106(4)	113.49	O3–C13–O4	123.11(14)	122.47
C6–C7–H7	116(3)	117.38	H7–O7–C14	107.9(14)	106.16
C7–C7–H7	117(4)	120.89	O7–C14–O6	123.28(13)	122.15
C7–C6–O2	122.9(3)	125.04	H1W–O1W–H2W	103(2)	102.56
C7–C6–O1	112.9(3)	110.93	H2N–N2–H3N	121.5(19)	120.85
N2–C2–N1	121.4(3)	122.03	N2–C2–N1	121.53(13)	122.85
N1–C2–N3	110.7(3)	110.71	H1N–N1–C2	125.5(14)	124.15
C2–N3–C3	127.5(3)	125.49	N3–C2–N1	110.58(13)	110.93
C2–N3–C4	110.1(3)	109.83	C2–N3–C4	109.95(12)	109.69
C4–C5–N1	107.2(3)	105.13	N1–C5–C4	106.50(12)	105.53
C5–N1–C2	109.8(3)	111.13	N1–C5–O5	124.85(13)	127.5
C4–C5–O5	128.1(3)	127.08	C2–N3–C3	127(13)	125.65
N1–C5–O5	124.8(3)	127.61	H4–C4–H44	109.2(14)	108.97
H3N–N2–H2N	127(5)	120.34	H2C–C3–H1C	109.5(16)	108.74
C2–N1–H1N	131(3)	121.11			
C2–N2–H2N	114(3)	119.69			
C2–N2–H3N	119(4)	124.67			
Torsion angles (°)			**Torsion angles (°)**		
			O2–C6–C7–C8	−4.2(2)	−0.504
O3–C8–C9–C9	−167.3(4)	−171.99	O1–C6–C7–C8	175.79(13)	179.71
O4–C8–C9–C9	11.9(7)	11.01	O3–C13–C9–C8	2.3(2)	3.86
O1–C6–C7–C7	−176.7(6)	−179.92	O4–C13–C9–C8	−176.48(14)	−176.42
N2–C2–N3–C3	−1.0(6)	−0.27	O4–C13–C9–C10	1.8(2)	3.53
N2–C2–N3–C4	177.91(3)	176.66	N1–C2–N3–C3	165.89(14)	175.65
C2–N1–C5–O5	−179.3(4)	−179.69	N1–C2–N3–C4	1.35(17)	3.16
N2–C2–N1–C5	−178.6(3)	−178.32	C2–N1–C5–O5	177.66(13)	179.32
C3–N3–C4–C5	1.5(4)	−175.05	N3–C4–C5–O5	−177.05(14)	−177.64

compounds the strongest interactions are established between anions and are of type O–H···O (2.555(4) Å (**I**) and 2. 2.5699(15) Å (**II**)) parallel to the crystallographic ***b***-axis. The creatininium entities in (**I**) are connected to each other via one N–H···O hydrogen bond, while this interaction is absent in (**II**). In addition cations and anions in (**II**) are connected via one strong O–H···O hydrogen bond unlike (**I**) where we note the absence of this interaction.

Hence, the crystal structure of (**I**) and (**II**) was stabilized by strong N–H···O and O–H···O together with weak C–H···O intermolecular interactions. In (**I**) and (**II**) the five membered ring of the creatininium cation is planar; the bond distances and planarity of creatininium cations explain a resonance in imidazolyl ring and change distribution around N1atom (protonation site).

3.2. DFT quantum chemical calculations

To investigate the molecular structures of (**I**) and (**II**), quantum mechanical calculations were carried out using density functional

Table 5
Values of the vibration wave numbers (cm^{-1}) of (**I**) and (**II**) calculated using experimental and DFT methods.

Compound (I)				Compound (II)			
Assignments	Infrared ν/cm^{-1} DFT	Infrared ν/cm^{-1} Exp	Raman ν/cm^{-1} Exp	Assignments	Infrared ν/cm^{-1} DFT	Infrared ν/cm^{-1} Exp	Raman ν/cm^{-1} Exp
O–H and C–O(H) str., N–H ….O str.	3333.9	3333.9		O–H & C–O(H) str.; N–H···O str.	3531.3	3522.1	3104.5
NH_2asym. str.	3085.16	3080.5	3089.0	NH_2asym. str.	3109.6	3102.3	3069.5
NH_2 sym. str.			3046.5	NH_2 sym. str.; Aromatic C–H str.	3008.6	3002.5	3049.0
CH_3 sym str.	2952.1	2949.5	2959.0	CH_3asym str.; (C)O–H str.			2987.5
CH_2asym str. N–H…O str	2923.7	2921.2	2925.5	CH_3 sym str.			2958.5
NH sym. str., N–H···O str., C–N asym. str.			2885.0	CH_2asym str. N–H···O str			2931.0
				CH_2asym str.			2825.5
C=O str. C–H asy. str. combi.	1760.3	1748.4	1743.5	C=O & O–H str.	2781.3	2776.7	2647.9
C–N asym. str. C=O str., C–C str.			1716.0	C=O str., C–N asym. str.	1741,2	1736.0	
NH_2asy. def.; O-H i.p.bend; C–N str.; C=O str.	1686.5	1681.4	1669.5	NH_2 sciss, C–N str., C=O str.	1710.8	1704.8	1691.5
C=C str.			1612.5	C=O str.	1699.5	1693.2	
				CH_2 rock, C=O str.	1620.4	1612.1	
COO^-asym. str; NH_2 sym def.	1572.7	1572.7	1476.5	C–N asym. str., COO^-asym. str.	1559.1	1554.6	1601.2
CH_2 twist			1430.1	CH_2 wagging, C–H def.	1507.2	1500.2	1431.7
O-H i.p.bend, C-H i.ph.bend.	1420.1	1417.4	1398.0	C–N asym str.; CH_2 rock.	1460,1	1454.0	
C–C asym., CH_3 sym. def., CH_2 wag.	1381.2	1376.6	1344.0	CH_3 sym def.; CH_2 wag; O–H i.p. def.	1372,5	1368.5	
C–N sym. str.			1304.5	C–N sym. str.	1272.0	1268.0	
C–C asy. str.			1276.1	C=N str.	1251,8	1248.2	
CH_2 twist	1279.8	1273.7	1229.5	CH_2 rock.			1189.5
C–H def.			1203.5	C–N str.; aromatic C–H bend.	1183,1	1174.0	1125.5
C–OH i.p.def.				C–O str.	1108,6	1104.0	
NH_2 rock	1167,1	1162	1039.2	C–C–N asym str.; CH_2 wag.	1044,2	1040.0	1002.0
C–N sym. str., CH_3 rock	1011.6	1006.1	973.5	C–N sym Str.; CH_3 rock.			
C–H i.ph.bend.	972.3	956.5	901.5	CH str.	980,7	978.0	
C–C sym. str.				C – C – N sym str.	889,2	882.1	840.0
C-H i.ph.bend.	882.4	873.1	828.5	Aromatic C–H bend.;H_2O rock.	842,1	836.2	
C – C str.			768.5	Aromatic C–H bend.	789,5	776.0	769.2
C=O sym	798.9	795.7	720.5	C–N–C str.; C–C–C str.	675,2	670.2	654.3
C=O sym	777.1	774.4	650.2	O–C=O i.p. def.; NH i.ph. bend.	610,2	600.6	599.0
CH_2 rock			597.0	CH_2twist.; COO^- wag.	601,3	574.0	385.0
C=O asym., C–H i.p.bend	691	686.0	566.1	COO^- rock.	536.0	520.0	370.0
C–C=C i.p.bend.	642.5	634.6	458.5	Ring breathing; OH str.			363.1
C–C=O def.	601.2	597.3	411.5	Ring breathing			319.0
COO^- wag	560.4	555.7	366.0	C–C–C–C. o.ph. def.			225.0
COO^- rock	448.1	445.5	316.5	Lattice vibration			128.0
C–C–C–C i. ph. def.			282.2				101.2
C–N def.			163.0				77.5
Lattice vibration			105.3				60.2

- **str.**: stretching; **sym. str.**; symmetric stretching; **asym. str.**; asymmetric stretching; **i.p.def.**; in phase deformation; **asy. str. combi.**; asymmetric stretching combination; **asy. def.**; asymmetric deformation; **i.p.bend.**; in plane bending; **wag.**; wagging.

theory (DFT) at the B3LYP/6-311 + G(d,p) level of theory. The calculated values of bond lengths, bond angles, and dihedral angles for (**I**) and (**II**) were compared with experimental values obtained by X-ray diffraction. Table 4 summarizes the experimental and optimized geometric parameters of (**I**) and (**II**) at the B3LYP/6-311G level using the atom numbering scheme in Figs. 1a and 3a. The obtained results showed good agreement between optimized geometric parameters and structural experimental values. Figs. 1b and 3b shows the optimized geometries of the most stable structures of (**I**) and (**II**), which both exhibit C1 symmetry.

It is important to note that the small differences between the calculated and observed geometrical parameters can be explained by the fact that the theoretical calculations were performed with isolated molecules in the gaseous phase while the experimental values have been based on the molecules in the solid state (crystalline state).

3.3. Analysis of vibrational spectra

Compound (**I**) consists of 38 atoms and compound (**II**) of 39 atoms having 108 and 111 normal modes of vibration for (**I**) and (**II**) respectively. All vibrational modes of the title molecule are IR active because the molecules possess C1 point group symmetry. All the experimental and theoretical vibrational frequencies of the title molecules, along with corresponding vibrational assignments and intensities are given in Table 5. In general, the computed vibrational frequencies are in excellent agreement with accurate experimental data and are compared with the values found in the literature [45].

FTIR and RAMAN spectra have been used to analysis the chemical bonding and structures (Fig. 5) and they consist of characteristic bands of different functional groups like N–H···O, C–N, COO^-, C–C, C–H, benzene ring, etc. The intermolecular hydrogen bond N–H···O appear in the region 2921.2 cm^{-1} in the IR of spectra for (**I**). The corresponding vibration is observed at 2952.5, 2931 cm^{-1} in Raman spectra for (**I**) and (**II**) respectively. The C–N stretching vibration is occurred at 1681.4, 1704.8 cm^{-1} for (**I**) and (**II**) respectively in IR spectra and 1669.5, 1691 cm^{-1} for (**I**) and (**II**) in Raman spectra. In the present study, the band at 1681.4 cm^{-1} for (**I**) in IR spectrum and 1669.5 cm^{-1} in Raman spectrum is due to O–H in-plane bending vibration. The band at 1417.4 cm^{-1} in IR spectrum and 1430 cm^{-1} in Raman spectrum of (**I**) is assigned to the O–H in-plane bending vibration mixed with C–H in-plane bending vibration. The ionized carboxylic group COO^- asymmetric stretching observed at 1572.7 cm^{-1} in Infrared spectrum of (**I**) (Fig. 5). Likewise, the characteristic vibrations of the amine group within the compound (**II**) appear at 3102.3 cm^{-1} in IR spectra

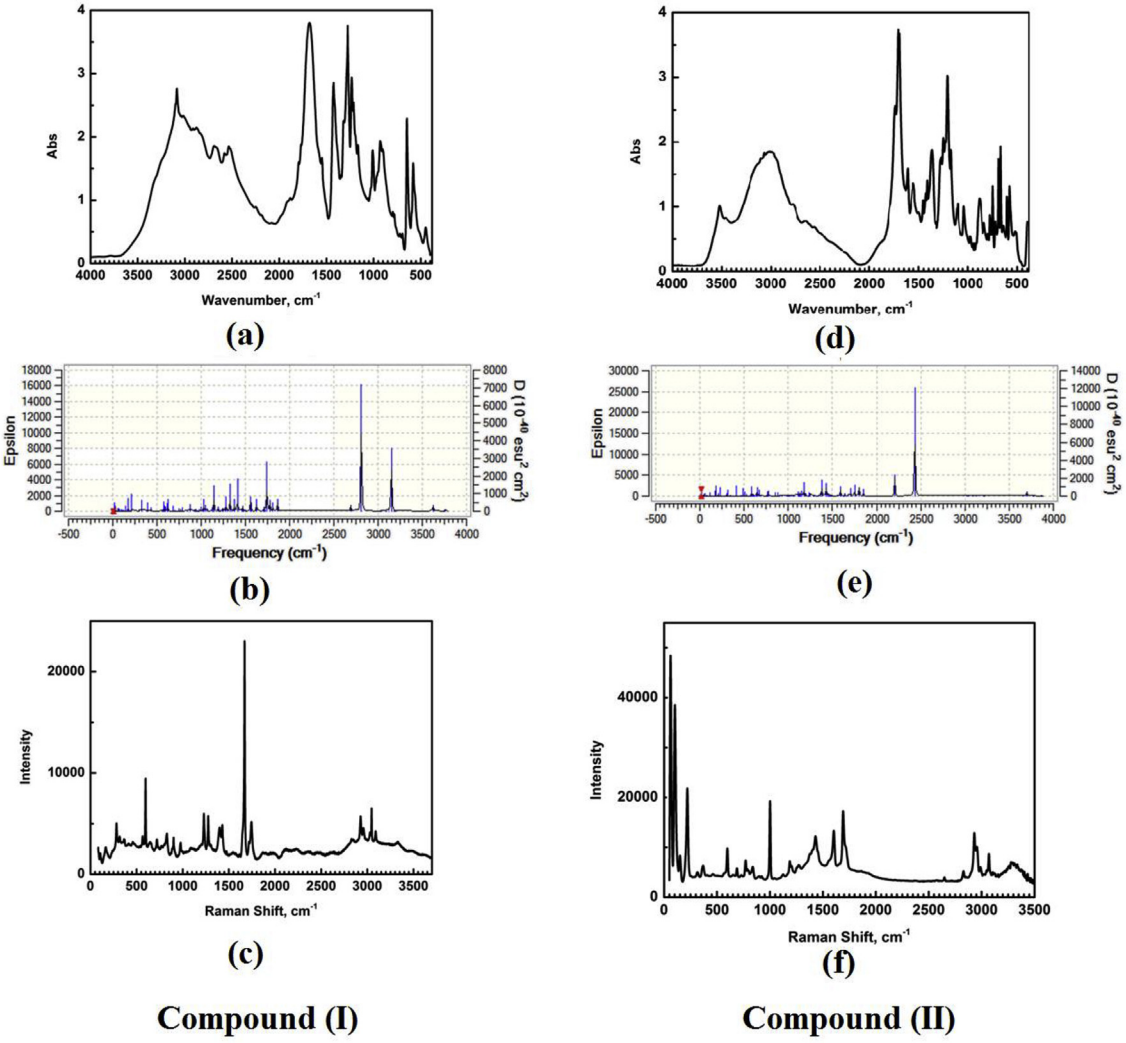

Fig. 5. (**a**) Experimental and (**b**) theoretical IR spectra of (**I**) and (**c**) Raman spectra of (**I**). (**d**) Experimental and (**e**) theoretical IR spectra of (**II**) and (**f**) Raman spectra of (**II**).

and 3069 cm^{-1} in Raman spectrum. Furthermore, the carboxylate group gives rise to a COO^{-} asymmetric stretching in the IR spectrum of (**II**) at 1554.6 cm^{-1} in IR spectra and 1601.2 cm^{-1} in Raman spectrum. The rocking mode occurs at 520 cm^{-1} in IR spectra and the wagging mode appears at 574 cm^{-1} and the scissoring deformation mode is identified at 642.5 cm^{-1} in IR spectrum. Concerning the O–C=O in-plane deformation mode, it was observed at 600 cm^{-1} in IR spectrum and 599 cm^{-1} in Raman spectrum of (**II**). The spectral data and the bands assignment for (**I**) and (**II**) are shown in Table 5.

3.4. Study of intermolecular interactions by Hirshfeld surface analysis

The Hirshfeld surfaces of (**I**) and (**II**) were mapped over d_{norm} (0.5–1.5 Å) and are illustrated in Fig. 6. The red circular depressions visible in the front and back surface views indicate hydrogen bonding contacts. The strongest and shortest interactions are due to N–H···O [N2–H3N···O5, N2–H2N···O3, N1–H1N···O4, N2–H3N···O5 for **(I)** and N2–H1N···O1W for **(II)**] and O–H···O [O1–H1···O3 for **(I)** and O7–H7···O5, O1W–H2W···O4, O3–H3···O1 for **(II)**] hydrogen bonds manifest in the Hirshfeld surfaces as the six (06) and the eight(8) bright red areas for (**I**) and (**II**) respectively. The other visible spots on the surfaces correspond to weak C–H···O hydrogen bonds. So, the color intensity exhibits the intensity of interaction.

Figs. 7 and 8 depict Hirshfeld surface fingerprint plots and percentage contributions of various intermolecular contacts for structures (**I**) and (**II**), respectively. The decomposed fingerprint plots exhibited in these figures include the reciprocal X···H/H···X contacts in which X atom is located inside (for X···H/$d_e < d_i$) or outside (for H···X/$d_e > d_i$) the generated *HS* as an H-atom acceptor.

For both structures, O···H/H···O contacts, which are attributed to N–H···O and O–H···O hydrogen-bonding interactions, appear as two sharp symmetric spikes in the two dimensional fingerprint maps (Figs. 7b and 8b respectively). They have the most significant contribution to the total Hirshfeld surfaces, with a percent of 44.4% (**I**) and 44.3% (**II**). The presence of these long spikes characteristic of strong hydrogen bonds which exhibits the shortest contacts at *ca* 1.58 Å for (**I**) (Fig. 7b) and at *ca* 1.64 Å for (**II**) (Fig. 8b) associated with the anion–anion interactions O1–H1···O3 (**I**) and O3–H3···O1 (**II**). Furthermore, in (**II**) there are other cation-anion interactions O7–H7···O5 (and its reciprocal O5···H7–O7) which represent the second shortest contact at *ca* 1.67 Å. The cation–cation interactions in (**I**) N2–H3N···O5 (and its reciprocal O5···N3H–N2) have a short distance of about 1.85 Å (Fig. 7b).

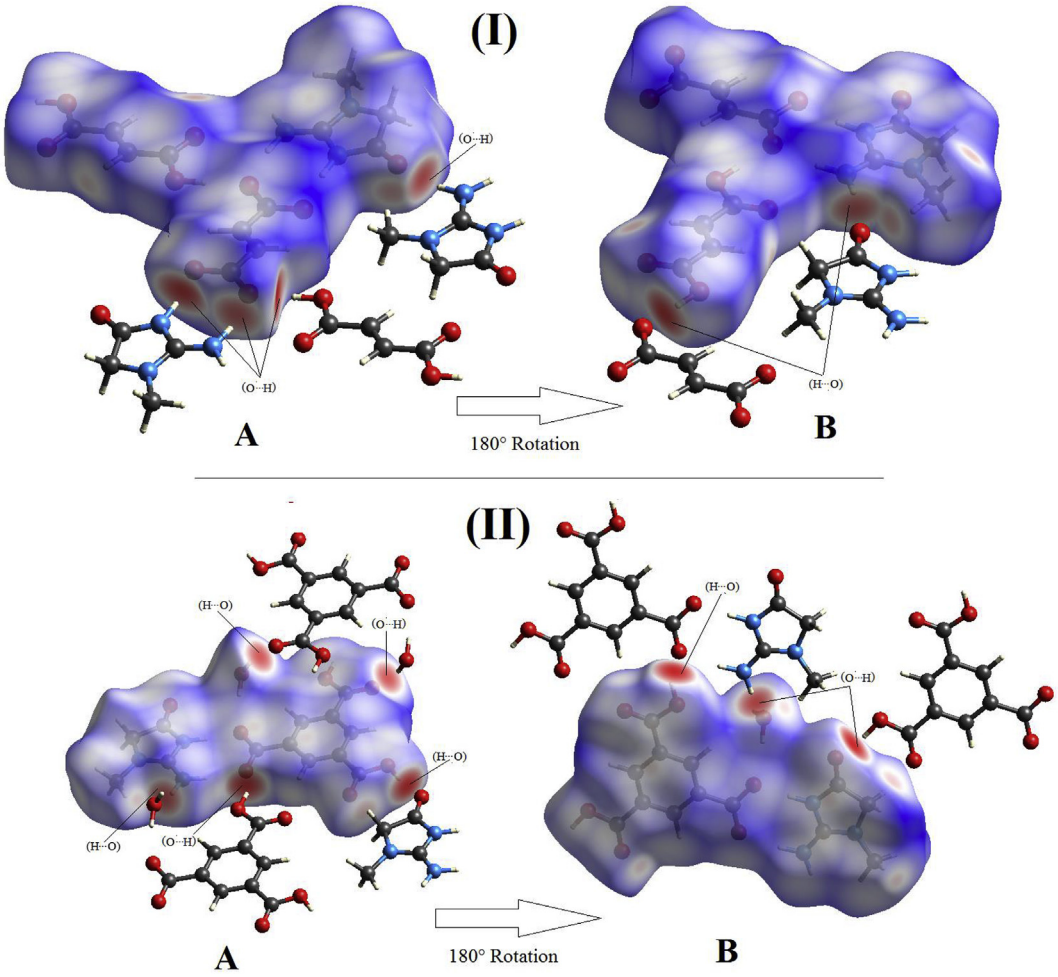

Fig. 6. 3D Hirshfeld maps with d_{norm} in the range 0.5–1.5 Å: **A**: front view and **B** back view. Red circle indicating short hydrogen bonds.

The H···H contacts appear in the middle of the scattered points in the two-dimensional fingerprint maps. In the two cases, they were found to be the second highest contributors towards the Hirshfeld surface, after the H···O/O···H contacts, covering 30.0% (Figs. 7c) and 25.4% (Fig. 8c) of the total surfaces for (**I**) and (**II**) respectively. Moreover, the fingerprint plot of (**II**) displays the presence of the shortest H···H contacts at *ca* 2.25 Å, attributed to O3–H3···H2N–N2 interaction (resulting from the hydrogen of the carboxyl group and the hydrogen of the amino group) and its reciprocal interaction N2–H2N···H3–O3 appearing in the 2D fingerprints at about $d_i = 1.25$ Å, $d_e = 0.98$ Å and $d_i = 0.98$ Å, $d_e = 1.28$ Å, respectively. In the case of (**I**), the spike on the d_e/d_i diagonal line is expanded because of the presence of several H···H interactions. Furthermore, the shortest H···H contact present within (**I**) assigned to the interaction C4–H4···H7–C7 (and its reciprocal C7–H7···H4–C4); it is built between the H4 hydrogen of the cation ring and the H7 hydrogen of the fumaric acid chain, and it is observed at *ca* 2.18 Å.

The decomposed fingerprint maps of C···H/H···C contacts appear as symmetrical wings in the fingerprint plots and include 12.0% of total Hirshfeld surface area for (**II**), whereas for (**I**) includes only 6.5% of the surface with the closest contacts at approximately 3.16 Å (Figs. 8d) and 2.98 Å (Fig. 7e), respectively. For (**II**) the contact result from the C5···H7/H7···C5 interactions between the C5 atom of creatinine ring and the H7 atom of carboxyl group, and for (**I**) it result from the C3–H3A···C8 hydrogen bonds between the H3A atom of the cation's methyl group and the C8 atom of the fumarate's carboxylate group.

The C···O and O···C contacts combined appear as a symmetric spike, on the top left ($d_e > d_i$,O···C) and bottom right ($d_e < d_i$, C···O) of the related plots in Figs. 7d and 8e, comprise 8.1% of the surface for (**I**) and 8.3% for (**II**).

Apart from the above interactions, the other C···C and N···H/H···N interactions are also observed. Furthermore, the C···C contacts assigned to the C5···C2/C2···C5 for (**I**) and C5···C9/C9···C5 for (**II**) which appear as stacking kite on the middle plot with minimum $d_i + d_e$ values of 3.35 Å for (**I**) and 3.27 Å for (**II**) as shown in Figs. 7f and 8f respectively.

The N···H/H···N contacts in (**I**) and (**II**) include only 2.8% and 3.0% respectively of the Hirshfeld surface. Such N···H/H···N contacts are included two spikes providing the closest contacts with minimum $d_i + d_e$ values near 3.24 Å attributed to the C3–H3A···N2 (and its reciprocal N2···H3A–C3) hydrogen bond for (**I**) and 2.68 Å attributed to the C3–H2C···N3 (and its reciprocal N3···H2C–C3) hydrogen bond for (**II**). In addition, the contacts of O···O, N···O/O···N and N···C/C···N are of low meaning as they are derived from less important interactions with small contributions in the all parts of Hirshfeld surface. The relative contributions of various intermolecular contacts to the Hirshfeld surface area in both compounds are shown in Fig. 9.

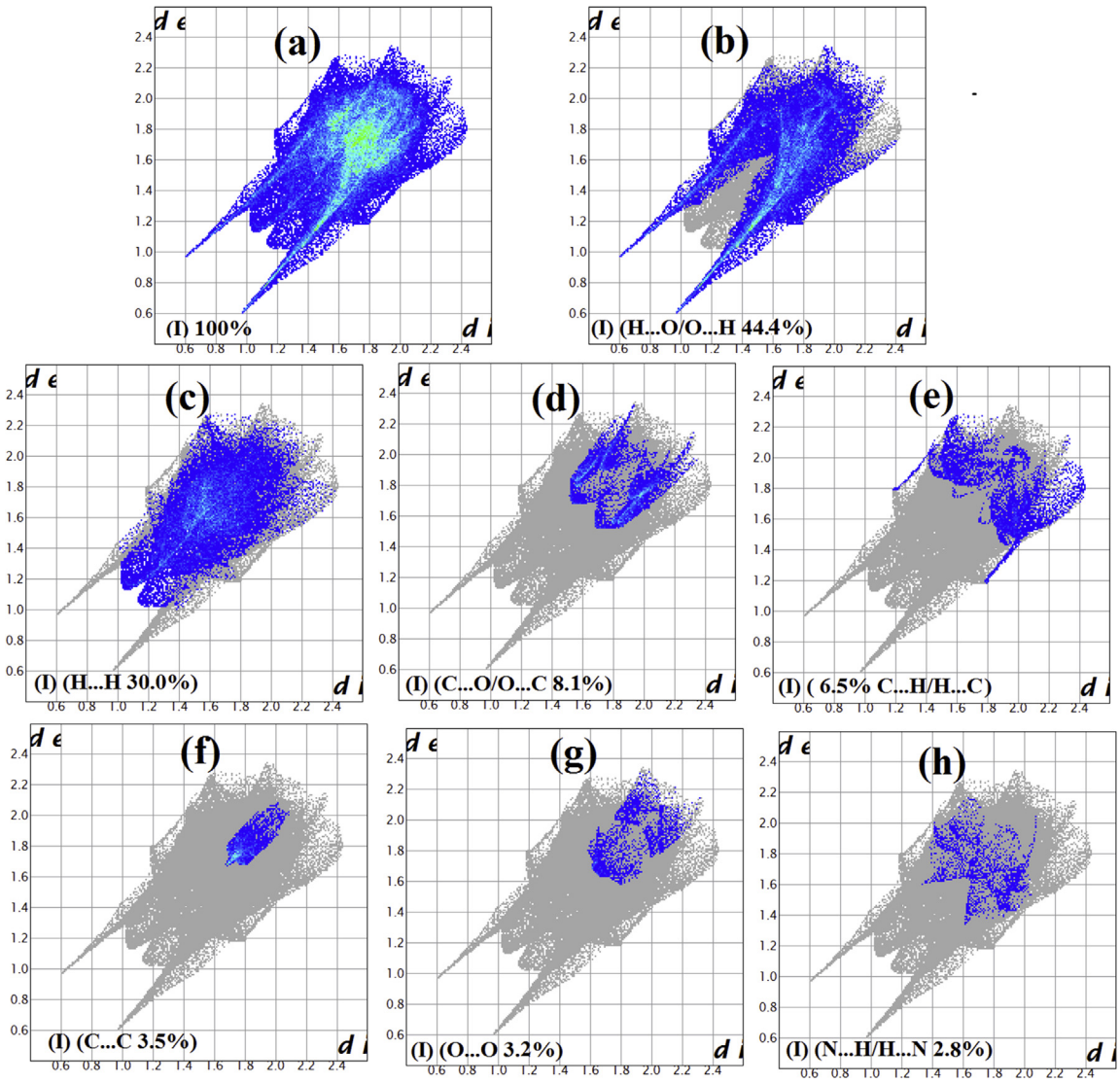

Fig. 7. 2D fingerprint plots of (**I**) showing percentages of contacts contributed to the total *HS* area.

This quantitative conclusion shows that the O···H/H···O interactions represent the important percentage of total surface in both compounds. Hence, these interactions constitute the driving force in crystal packings. The Hirshfeld surfaces certainly allow a detailed scrutiny by displaying all the intermolecular interactions within the crystal and this methodology has very important promise in crystal engineering.

3.5. Molecular orbital analysis

The obtained DFT results such as the highest occupied molecular orbital (HOMO), lowest unoccupied molecular orbital (LUMO) energies and their energy gaps (E_{gap}), at B3LYP/6-311 + G(d,p), for the compound (**I**) and (**II**) are presented in Table 6.

The HOMO-LUMO analysis was performed to visualize frontier molecular orbitals as well as to examine the charge transfer within the two compounds. These two parameters are imperative for determining and understanding how the molecules interact with other species (Fig. 10). HOMO, the outermost orbital containing electrons has a tendency to release electrons. On the other hand, LUMO orbital has free space to accept electrons. The ability of charge transfer interactions within molecule can be explained by the HOMO–LUMO energy gap [46,47]. The positive and negative phases are represented by red and green colors, respectively. The energy values correspond to HOMO and LUMO and their energy gap show the chemical activity and kinetic stability of the molecule. In Fig. 10 we note that HOMO orbital is delocalized to the coordinated part of creatininium while the LUMO orbital is delocalized to the fumaric acid in compound (**I**) and to the tricarboxylate acid in compound (**II**). The obtained results show that the HOMO-LUMO energy gap of compound **(I)** is slightly smaller than that for compound **(II)**, indicating therefore that the molecular structure of compound **(I)** is more favourable for charge transfer than that of compound **(II)**. These results are in good agreement with the Hirshfeld analyses which shows that the contributions of the O···H and H···H interactions to the crystal packing are greater for compound **(I)**.

4. Conclusion

In summary, we have reported in this work the synthesis, structural characterization, vibrational spectroscopy and DFT

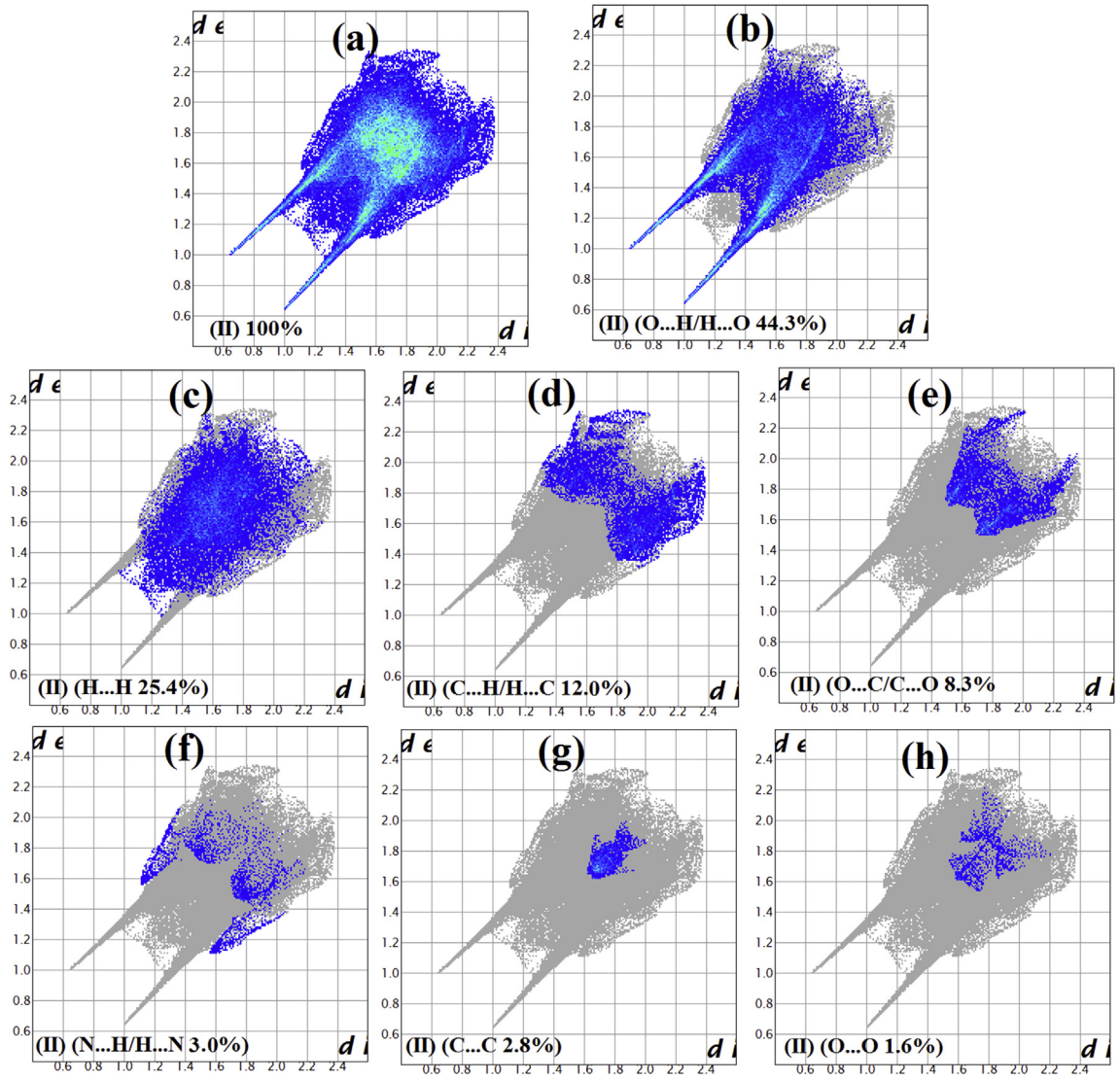

Fig. 8. 2D fingerprint plots of (**II**) showing percentages of contacts contributed to the total *HS* area.

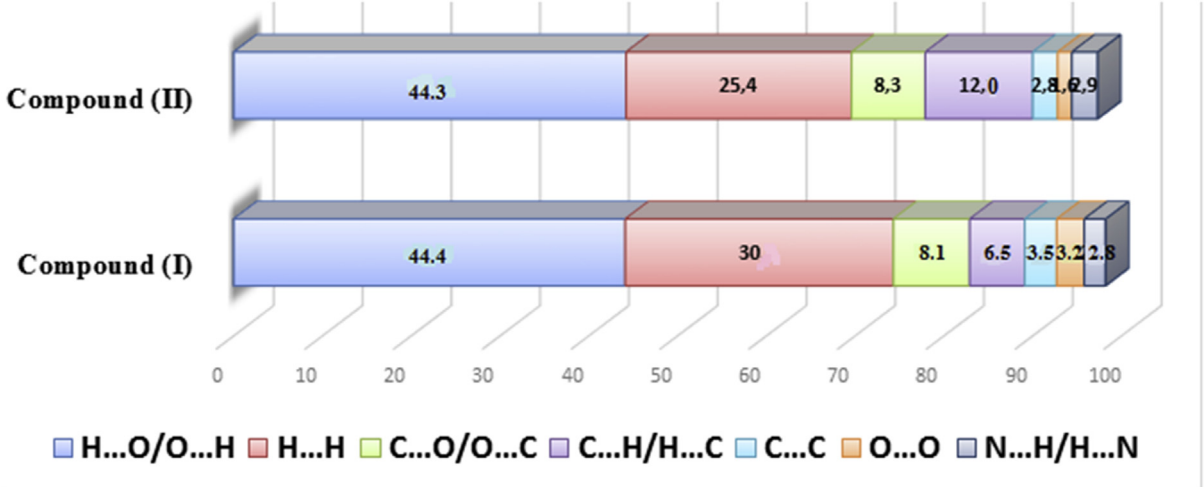

Fig. 9. Relative percentage contributions to the *HS* area for various intermolecular contacts for (**I**) and (**II**).

Table 6
HOMO-LUMO energy values calculated by DFT/B3LYP/6-311 + G(d,p).

Parameters	DFT/B3LYP/6-311 + G(d,p)
Compound (I)	
Total energy (ua)	−1307,3593
E_{HOMO} (eV)	−0,33789
E_{LUMO} (eV)	−0,23287
$\Delta E_{HOMO\text{-}LUMO\ gap}$ (eV)	0,10502
Compound (II)	
Total energy (ua)	−1270,9231
E_{HOMO} (eV)	−0,33699
E_{LUMO} (eV)	−0,22473
$\Delta E_{HOMO\text{-}LUMO\ gap}$ (eV)	0,11226

calculation of bis (creatininium) fumarate fumaric acid (**I**) and creatininium 3,5-dicarboxybenzoate monohydrate (**II**). Both crystals are centrosymmetric and belongs to monoclinic ($P2_1/c$) and triclinic (P-1) systems for (**I**) and (**II**) respectively. The calculated geometrical parameters, using of B3LYP/6-311 + G(d,p), are in good agreement with the experimental values obtained from the crystallographic data. All the vibrational wavenumbers are calculated and scaled values are compared with experimental FT-IR and Raman spectra. Experimentally observed frequencies are in good agreement with the calculated values. The Hirshfeld surface analysis coupled with the structural investigation reveal that crystal packing of both compounds is characterized by a three-dimensional network of hydrogen bonds and the main contributions are provided by the O···H/H···O and H···H interactions, which alone represent ~75% for (**I**) and ~70% for (**II**) of the total contributions to the Hirshfeld surfaces. These findings are in good agreements with the molecular orbital analysis results which show that the HOMO-LUMO energy gap of compound **(I)** is slightly smaller than that for compound **(II)**, indicating therefore that the molecular structure of compound **(I)** is more favourable for charge transfer than that of compound **(II)**.

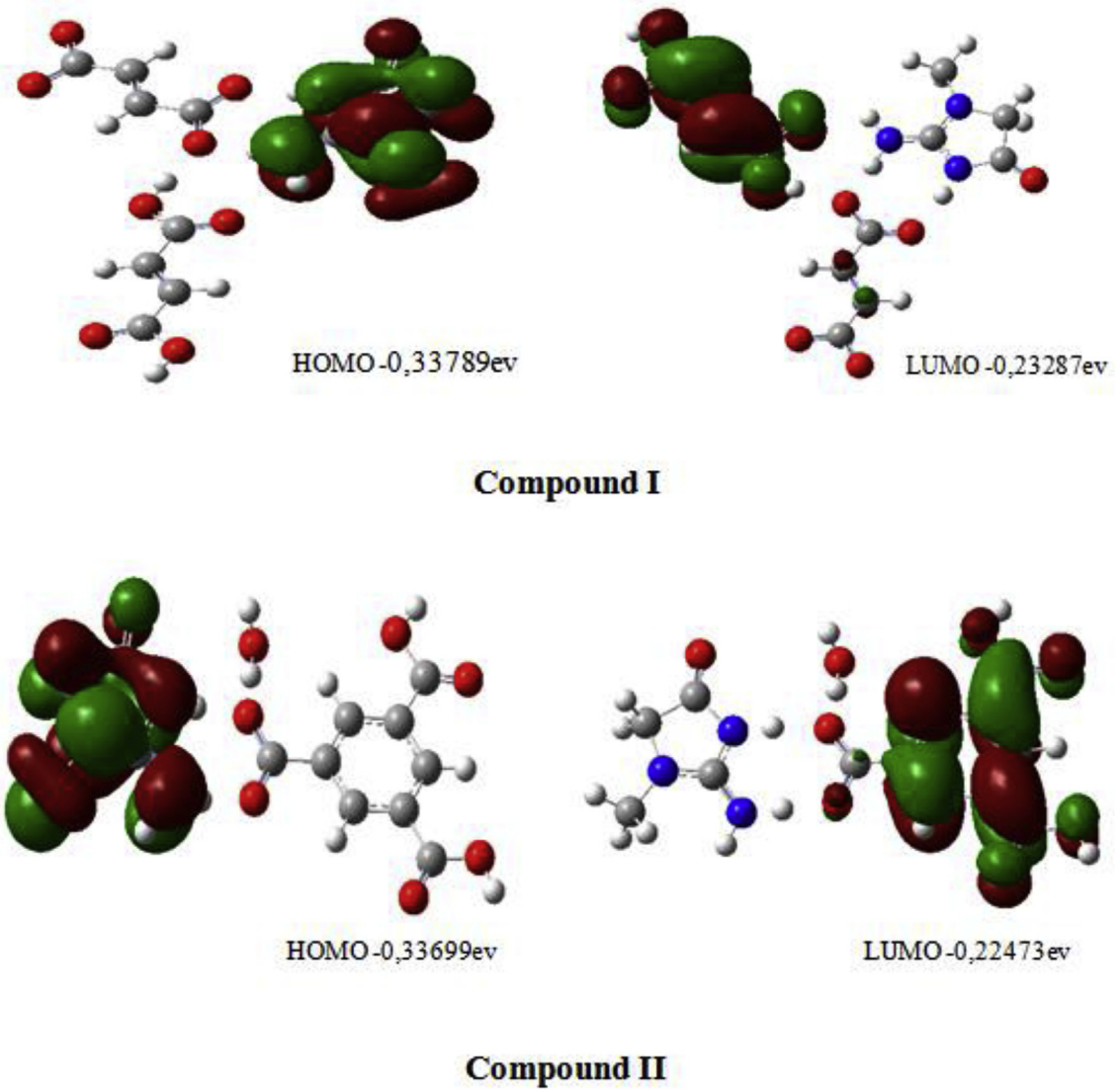

Fig. 10. Frontier molecular orbitals (HOMO and LUMO) of (**I**) (top) and (**II**) (bottom).

Acknowledgements

This work was financially supported by the University 'Abbes Laghrour', Khenchela (Algeria). W. Falek gratefully acknowledges Professor D. Luneau and Mr. G. Pilet from University of Claude Bernard Lyon 1 for providing diffraction facilities and to the X-Ray diffraction platform of the Institut Jean Barriol (University of Lorraine) for complementary structural analysis.

Appendix A. Supplementary data

Supplementary data to this article can be found online at https://doi.org/10.1016/j.molstruc.2019.04.084.

References

[1] V. Thayanithi, P. Praveen Kumar, B. Gunasekaran, IUCrData 1, 2016, p. x160989.
[2] T.L. Wang, H.K. Chiang, H.H. Lu, F.Y. Peng, Opt. Quant. Electron. 37 (2005) 1415–1422.
[3] N.M. Settergren, P. Buhlmann, E.A. Amin, J. Mol. Struct. Theochem. 861 (2008) 68–73.
[4] M. Nagasaka, H. Kondoh, K. Amemiya, T. Ohta, Y. Iwasawa, Proton transfer in waterehydroxyl mixed overlayers on Pt (111): combined approach of laser desorption and spatially-resolved X-ray photoelectron spectroscopy, Surf. Sci. 603 (10) (2009) 1690–1695.
[5] R. Thirumurugan, B. Babu, K. Anitha, J. Chandrasekaran, J. Mol. Struct. 1149 (2017) 48–57.
[6] R. Thirumurugan, B. Babu, K. Anitha, J. Chandrasekaran, Mater. Lett. 185 (2016) 214–217.
[7] R. Thirumurugan, K. Anitha, J. Mol. Struct. 1146 (2017) 273–284.
[8] R. Thirumurugan, B. Babu, K. Anitha, J. Chandrasekaran, Optic Laser. Technol. 105 (2018) 106–113.
[9] R. Thirumurugan, K. Anitha, Mater. Lett. 206 (2017) 30–33.
[10] M.K. Kumar, S. Sudhahar, P. Pandi, G. Bhagavannarayana, R.M. Kumar, Opt. Mater. 36 (2014) 988–995.
[11] C.R. Groom, I.J. Bruno, M.P. Lightfoot, S.C. Ward, Acta Crystallogr. B 72 (2016) 171–179.
[12] C. Ramachandra Raja, A. Antony Joseph, Mater. Lett. 63 (2009) 2507–2509.
[13] A. Arunkumar, P. Ramasamy, Mater. Lett. 123 (2014) 246–249.
[14] M. Rajkumar, M. Saravanabhavan, A. Chandramohan, Opt. Mater. 72 (2017) 247–256.
[15] M.C. Burla, R. Caliandro, M. Camalli, B. Carrozzini, G.L. Cascarano, C. Giacovazzo, M. Mellamo, G. Polidori, R. Spagna, J. Appl. Crystallogr. 49 (2012) 357–361.
[16] G.M. Sheldrick, Acta Crystallogr. A 71 (2015) 3–8.
[17] L.J. Farrugia, J. Appl. Crystallogr. 45 (2012) 849–854.
[18] C.F. Macrae, P.R. Edgington, P. McCabe, E. Pidcock, G.P. Shields, R. Taylor, M. Towler, J. van de Streek, J. Appl. Crystallogr. 39 (2006) 453–457.
[19] J.K. Labanowski, J.W. Andzelm, Density Functional Methods in Chemistry, Springer Verlag, New York, 1991.
[20] J. Baker, An algorithm for the location of transition states, J. Comput. Chem. 7 (1986) 385–395.
[21] H.B. Schlegel (Ed.), Modern Electronic Structure Theory: GeometryOptimization on Potential Energy Surfaces, World Scientific, Singapore, 1994.
[22] W.J. Hehre, L. Radom, P.V.R. Schleyer, J.A. Pople, Ab Initio Molecular Orbital Theory, Wiley, New York, 1986.
[23] P.C. Hariharan, J.A. Pople, The influence of polarization functions on molecular orbital hydrogenation energies, Theor. Chim. Acta 28 (1973) 213–222.
[24] A. Becke, Density-functional exchange-energy approximation with correct asymptotic behavior, Phys. Rev. A 38 (1988) 3098–3100.
[25] A.D. Becke, A new mixing of HartreeeFock and local densityfunctional theories, J. Chem. Phys. 98 (1993) 1372–1377.
[26] C. Lee, W. Yang, R.G. Parr, Development of the ColleeSalvetti correlation-energy formula into a functional of the electron density, Phys. Rev. B 37 (1988) 785–789.
[27] M.J. Frisch, G.W. Trucks, H.B. Schlegel, G.E. Scuseria, M.A. Robb, J.R. Cheeseman, J.A. Montgomery, J. Vreven, T. Kudin, K.N. Burant, J.C. Millam, J.M. Iyengar, S.S. Tomasi, J. Barone, V. Mennucci, B. Cossi, M. Scalmani, G. Rega, N. Petersson, G.A. Nakatsuji, H. Hada, M. Ehara, M. Toyota, K. Fukuda, R. Hasegawa, J. Ishida, M. Nakajima, T. Honda, Y. Kitao, O. Nakai, H. Klene, M. Li, X. Knox, J.E. Hratchian, H.P. Cross, J.B. Adamo, C. Jaramillo, J. Gomperts, R. Stratmann, R.E. Yazyev, O. Austin, A.J. Cammi, R. Pomelli, C. Ochterski, J.W. Ayala, P.Y. Morokuma, K. Voth, G.A. Salvador, P. Dannenberg, J.J. Zakrzewski, V.G. Dapprich, S. Daniels, A.D. Strain, M.C. Farkas, O. Malick, D.K. Rabuck, A.D. Raghavachari, K. Foresman, J.B. Ortiz, J.V. Cui, Q. Baboul, A.G. Clifford, S. Cioslowski, J. Stefanov, B.B. Liu, G. Liashenko, A. Piskorz, P. Komaromi, I. Martin, R.L. Fox, D.J. Keih, T. Al-Laham, M.A. Peng, C.Y. Nanayakkara, A. Challacombe, M. Gill, P.M.W. Johnson, B. Chen, W. Wong, M.W. Gonzalez, C. Pople, Gaussian 03, Gaussian Inc., Pittsburg, PA, 2003.
[28] J.A. Montgomery, M.J. Frisch, J.W. Ochterski, G.A. Peterson, J. Chem. Phys. 110 (1999) 2822–2827.
[29] A. Cavalli, P. Carloni, M. Recanatini, Chem. Rev. 106 (2006) 3497–3519.
[30] M.A. Spackman, J.J. McKinnon, CrystEngComm 4 (2002) 378–392.
[31] M.A. Spackman, P.G. Byrom, Chem. Phys. Lett. 267 (1997) 215–220.
[32] J.J. Mckinnon, M.A. Spackman, A.S. Mitchell, Acta Crystallogr. B 60 (2004) 627–668.
[33] S.K. Wolff, D.J. Grimwood, J.J. McKinnon, M.J. Turner, D. Jayatilaka, M.A. Spackman, CrystalExplorer, Version 3.1, University of Western Australia, Perth, 2012.
[34] A. Jahubar Ali, S. Athimoolam, S. Asath Bahadur, Acta Crystallogr. 67 (2011) 2905.
[35] H.S. Wilkinson, W.T.A. Harrison, Acta Cryst.E 61 (2005) 1228–1230.
[36] T. Guinovart, D. Hernandez-Alonso, L. Adriaenssens, P. Blondeau, M.M. Belmonte, F.X. Rius, F.J. Andrade, P. Ballester, Angew. Chem. Int. Ed. 55 (2016) 2435–2440.
[37] J. Bernstein, R.E. Davis, L. Shimoni, N.L. Chang, Angew Chem. Int. Ed. Engl. 34 (1995) 1555–1573.
[38] M. Hemamalini, H.K. Fun, Acta Crystallogr. E66 (2010) 2093–2094.
[39] F.F. Said, B.F. Ali, D. Richeson, I. Korobkov, Acta Crystallogr. E 68 (2012) 1906.
[40] S. Dong, Y. Tao, X. Shen, Z. Pan, Acta Crystallogr. C 69 (2013) 896–900.
[41] S. Jin, Y. Zhao, B. Liu, X. Jin, H. Zhang, X. Wen, H. Liu, L. Jin, D. Wang, J. Mol. Struct. 1099 (2015) 601–615.
[42] C.B. Aakeröy, M.E. Fasulo, J. Desper, Mol. Pharm. 4 (2007) 317–322.
[43] S. Pré, H. Mendel, Acta Crystallogr. 8 (1955) 311–313.
[44] R. Thomas, G.U. Kulkarni, J. Mol. Struct. 873 (2008) 160–167.
[45] A. Jahubar Ali, S. Thangarasu, S. Athimoolam, S. Asath Bahadur, RJPBCS 4 (2013) 1292–1303.
[46] A.F. Jalbout, B. Trzaskowski, A.J. Hameed, J. Organomet. Chem. 691 (2006) 4589–4594.
[47] A.F. Jalbout, A.J. Hameed, B. Trzaskowski, J. Organomet. Chem. 692 (2007) 1039–1047.